

# Effects of correlated turbulent velocity fields on the formation of maser lines

R. Böger<sup>1</sup>, W.H. Kegel<sup>2,3</sup>, and M. Hegmann<sup>3</sup>

<sup>1</sup> Hamburger Sternwarte, Universität Hamburg, Gojenbergsweg 112, D-21029 Hamburg  
e-mail: rboeger@hs.uni-hamburg.de

<sup>2</sup> Institut für theoretische Physik der Universität Frankfurt am Main, Robert-Mayer Strasse 8-10,  
D-60054 Frankfurt am Main  
e-mail: kegel@astro.uni-frankfurt.de

<sup>3</sup> Zentrum für Astronomie und Astrophysik der Technischen Universität Berlin,  
Sekt. PN 8-1, Hardenbergstrasse 36, D-10623 Berlin  
e-mail: [hegmann,kegel]@astro.physik.tu-berlin.de

Received 19 February 2003 / Accepted 20 May 2003

**Abstract.** The microturbulent approximation of turbulent motions is widely used in radiative transfer calculations. Mainly motivated by its simple computational application it is probably in many cases an oversimplified treatment of the dynamical processes involved. This aspect is in particular important in the analysis of maser lines, since the strong amplification of radiation leads to a sensitive dependence of the radiation field on the overall velocity structure. To demonstrate the influence of large scale motions on the formation of maser lines we present a simple stochastic model which takes velocity correlations into account. For a quantitative analysis of correlation effects, we generate in a Monte Carlo simulation individual realizations of a turbulent velocity field along a line of sight. Depending on the size of the velocity correlation length we find huge deviations between the resulting random profiles in respect of line shape, intensity and position of single spectral components. Finally, we simulate the emission of extended maser sources. A qualitative comparison with observed masers associated with star forming regions shows that our model can reproduce the observed general spectral characteristics. We also investigate shortly, how the spectra are effected when a systematic velocity field (simulating expansion) is superposed on the fluctuations. Our results convincingly demonstrate that hydrodynamical motions are of great importance for the understanding of cosmic masers.

**Key words.** masers – radiative transfer – turbulence – line: formation

## 1. Introduction

Maser lines of various molecular species are observed in star forming regions and in the envelopes of evolved late type stars. In both cases it is well known that turbulent motions play an important role in the gas hydrodynamics. Their spectra show large velocity differences (up to tens of km/s) and are variable on observable time scales. VLBI-observations reveal that maser regions often consist of several isolated sources with different radial velocities (see, e.g., Reid et al. 1980). Due to the Doppler effect, the radiation field depends on the local velocity structure. This coupling to the velocity field does sensitively affect the formation of maser lines since in the unsaturated regime the radiation is exponentially amplified. To the extent that stochastic hydrodynamical velocities are involved, the correlation length, i.e., the length over which

the hydrodynamical velocity changes substantially, plays an important role. In the usual microturbulent analysis large scale motions are neglected. As a consequence, each spectral component will generally be attributed to a separate source and could in principle be formed under different physical conditions. The aim of the present investigation is to emphasize the necessity to consider hydrodynamical motions in more detail. We will show how correlated velocity fields affect the line forming process and that omitting this important aspect can lead to erroneous interpretations of observed maser spectra.

Traving and collaborators (Gail et al. 1974; Traving 1975) developed a theory allowing to account for correlated turbulent motions<sup>1</sup> in the transfer of line radiation.

<sup>1</sup> Here and in the following we use the term turbulence in the spectroscopic sense (which is wider than in hydrodynamics) referring to any stochastic motion leading to line broadening. The terms micro-, meso-, and macroturbulence refer to the

In their formalism, the hydrodynamic velocity  $v$  along a line of sight is described by a Markovian process defined by a Gaussian distribution function and an exponential correlation function. Due to the stochastic modeling of the velocity field, the intensity also has to be considered as a random variable. Traving showed that in accord with these assumptions and together with the usual equation of transfer, a Fokker-Planck equation can be derived, which describes the probability  $W(I_\nu, v, s)$  of finding at point  $s$ , the intensity  $I_\nu$  and the velocity  $v$ . Of particular interest is the expectation value of the intensity  $\langle I_\nu \rangle$  since it reflects as a time or spatial average the mean physical properties of the system. Gail et al. (1975) examined the model of an unsaturated maser applying the theory described above.

While this approach gives a first qualitative insight into the effects introduced by a turbulent velocity field, the question arises to which extent the calculated expectation value of the intensity may be directly compared with observed spectra. The answer depends in particular on two issues. The first is the question of how many statistically independent lines of sight contribute to a given observation. This obviously is a function of the spatial resolution. The second point is the question of how many spectra corresponding to individual lines of sight have to be averaged in order to obtain the expectation value with a certain accuracy. As will be shown later, in the case of unsaturated masers this number is very large. In order to investigate these questions we set up a Monte Carlo (MC) simulation scheme to generate individual realizations of the random velocity field. The calculated line profiles reflect the stochastic nature of the turbulent motion along a given line of sight and allow a quantitative analysis of correlation effects.

## 2. Model assumptions and the Monte Carlo method

In the case of an unsaturated maser the occupation numbers of the maser levels are essentially not affected by the intensity in the maser line. Consequently, the intensity variation along any line of sight depends just on the local physical conditions. In order to focus on the effect of correlated velocity fields, we assume a plane parallel slab with a homogeneous density and temperature distribution. Additionally, we take the velocity field to be quasi-static, presuming that the dynamical time scales are large in comparison with the duration of individual observations. The variation of the turbulent velocity along each line of sight is assumed to follow a Markov process and the projected velocity  $v(s)$  along a line of sight is treated as a random function of  $s$ . The one-point distribution function

---

way in which the turbulent motions affect the line broadening which depends on the ratio of the mean free path of a photon to the correlation length of the velocity field.

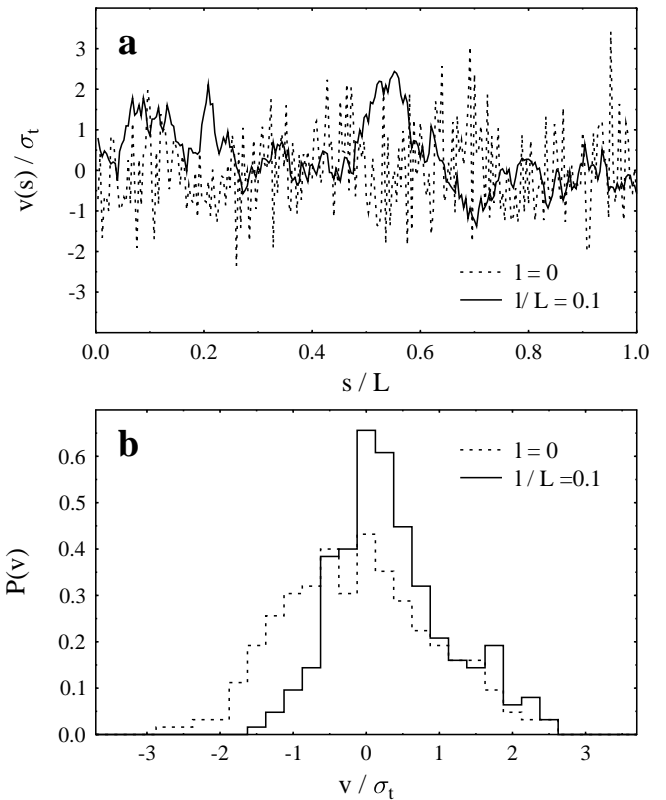


**Fig. 1.** (a) Individual realizations of the one-dimensional velocity field, and (b) the corresponding distribution function  $P(v)$  for the microturbulent ( $l = 0$ , dashed histogram) and a mesoturbulent ( $l/L = 0.1$ , solid histogram) model

of  $v$  is considered to be Gaussian with the rms turbulent velocity  $\sigma_t$

$$W(v) = \frac{1}{\sqrt{2\pi}\sigma_t} \cdot \exp\left[-\frac{v^2}{2\sigma_t^2}\right]. \quad (1)$$

The conditional probability of finding at point  $s + \Delta s$  the velocity  $v + \Delta v$  is

$$P(v + \Delta v, s + \Delta s | v, s) = \frac{1}{\sqrt{2\pi}\sigma_t^2(1-f^2)} \exp\left\{-\frac{[\Delta v + v(1-f)]^2}{2\sigma_t^2(1-f^2)}\right\} \quad (2)$$

with an exponential type correlation function

$$f(\Delta s) = \exp\left[-\frac{|\Delta s|}{l}\right]. \quad (3)$$

The correlation length  $l$  defines the length scale of the stochastic velocity variation. From Eq. (2) it follows that the expectation value of  $\Delta v$  is

$$\langle \Delta v \rangle = -v \left[ 1 - \exp\left(-\frac{|\Delta s|}{l}\right) \right] \quad (4)$$

and the variance is given by

$$\text{Var}(\Delta v) = \sigma_t^2 \left[ 1 - \exp\left(-\frac{2|\Delta s|}{l}\right) \right]. \quad (5)$$

The assumption that the variation of the velocity field along the line of sight may be described by a Markov process (implying an exponential correlation function) is the simplest way to introduce correlation effects into the theory of radiative transfer (see e.g. Gail et al. 1974, 1980). This assumption implies that only the one-point and the two-point distribution functions are important. All other correlation functions require the knowledge of higher order multi-point distribution functions. For later comparison with the work of others, we note that the (spatial) power spectrum of the velocity field is the Fourier transform of the correlation function. This means that (3) implies a one-dimensional power spectrum

$$P_1(k) \sim \frac{l}{1 + l^2 k^2} \quad (6)$$

which for  $l^2 k^2 \gg 1$  is well approximated by a power law,  $P(k) \sim k^{-2}$ . If we consider (3) as correlation function in three dimensions, i.e. if we consider  $s$  as a vector, we find for the three-dimensional power spectrum

$$P_3(k) \sim \frac{l}{(1 + l^2 k^2)^2} \quad (7)$$

The choice of the correlation function (3) makes it relatively easy to calculate individual realizations of the velocity field (see below), as well as the expectation value of the line profile using the generalized radiative transfer equation (Gail et al. 1974, 1975).

In accord with Eq. (2) the distribution of the random projected velocities can be generated in a Monte Carlo procedure (Levshakov et al. 1997):

$$v(s + \Delta s) = \xi \sqrt{\sigma_t^2 (1 - f^2)} + f v(s), \quad (8)$$

where  $\xi$  is a normally distributed random number with  $\langle \xi \rangle = 0$  and  $\text{Var}(\xi) = 1$ . The velocity at the edge of the cloud is given by  $v = \sigma_t \xi(s = 0)$ .

The line forming process depends sensitively on the ratio  $\sigma_t/v_{\text{th}}$  (see, e.g., Levshakov & Kegel 1994). In the case  $\sigma_t/v_{\text{th}} < 1$ , the line broadening is thermally dominated and the turbulent velocity correlation is insignificant. Contrary, if  $\sigma_t/v_{\text{th}} > 1$  correlation effects become pronounced. An inappropriately chosen step size can smear out the correlated structure of a random velocity field. This is avoided by satisfying the inequality

$$\text{Var}(\Delta v) < v_{\text{th}}^2. \quad (9)$$

From (5) it follows that for  $\sigma_t > v_{\text{th}}$  this is equivalent to

$$\frac{|\Delta s|}{l} \leq \ln \left[ 1 - (v_{\text{th}}/\sigma_t)^2 \right]^{-1/2}. \quad (10)$$

To illustrate the influence of a finite correlation length, Fig. 1 shows one realization of a completely uncorrelated (microturbulent) velocity field ( $l = 0$ , dashed line) and one realization of a mesoturbulent velocity field ( $l > 0$ , solid line). The lower panel represents the corresponding projected velocity distributions  $P(v)$ . As expected, the velocity in the limiting case is normally distributed, whereas

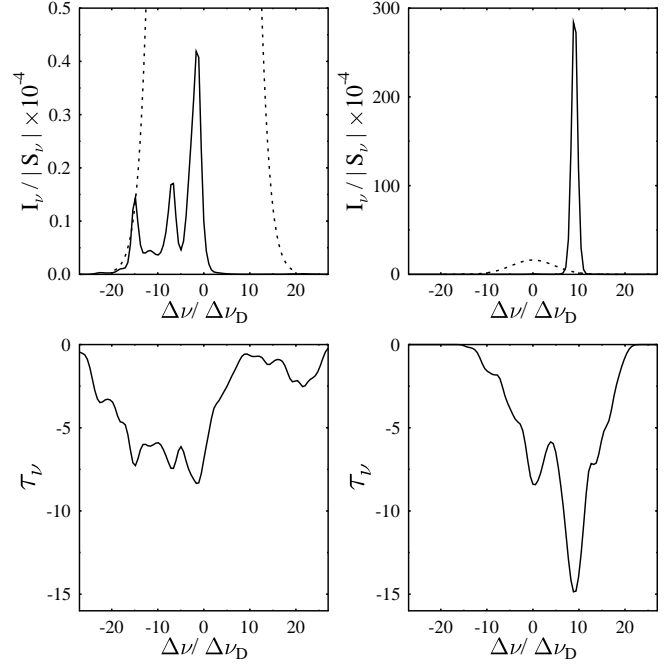


**Fig. 2.** Upper panels: Line profiles for two individual realizations of the velocity field (solid curve) for the parameter set  $l/L = 0.1$ ,  $\sigma_t/v_{\text{th}} = 10$ , and  $\tau_0 = -110$ . For comparison also the spectrum of the intensity expectation value is shown (dashed curve). Lower panels: The optical depth of the random spectra

the correlated velocity distribution deviates significantly from a Gaussian. This is due to the fact that for a finite ratio  $l/L$  the statistical base represents an incomplete statistical sample. Averaging over many realizations (either temporal or spatial) would yield an complete ensemble with a unique Gaussian distribution function. For simplicity, we neglect the dependence of the occupation numbers of the involved maser levels on the radiation in the maser line. If furthermore the source function  $S_\nu$  is assumed to be constant over the whole region, the equation of radiative transfer can be solved analytically. Neglecting the background radiation yields

$$I_\nu(s = 0) = S_\nu \{1 - \exp[-\tau_\nu(L)]\}, \quad (11)$$

with the optical depth

$$\tau_\nu(s) = \int_0^s \kappa_\nu ds', \quad (12)$$

and the monochromatic absorption coefficient

$$\kappa_\nu = \kappa_0 \Phi(\Delta\nu, v), \quad (13)$$

$\Phi(\Delta\nu, v)$  being the local profile function. It should be noted that for population inversion the source function and the absorption coefficient are both negative. If one considers thermal Doppler broadening as the dominant effect, the local profile function can be written as

$$\Phi(\Delta\nu, v) = \frac{1}{\sqrt{\pi} \Delta\nu_D} \cdot \exp \left\{ - \left[ \frac{(\nu - \nu_0)}{\Delta\nu_D} - \frac{v}{v_{\text{th}}} \right]^2 \right\}, \quad (14)$$

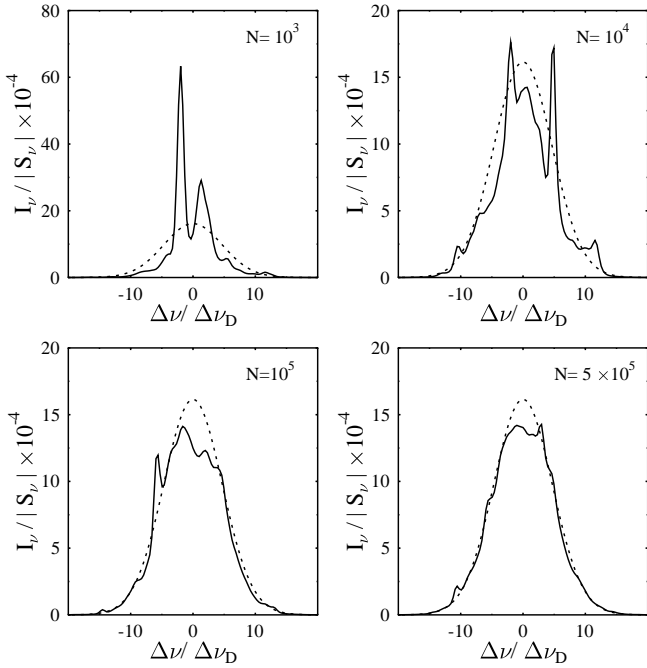


**Fig. 3.** Convergence of the ensemble average of  $N$  random profiles (solid line) to its expectation value (dashed line). The parameter configuration is the same as in Fig. 2

where  $\Delta\nu_D$  is the thermal Doppler width and  $v_{th}$  the thermal velocity. Equally, the projected random velocity distribution along a line of sight  $P(v)$  can be convolved with the thermal profile function to derive the optical depth

$$\tau_\nu(L) = \kappa_0 L \int_{-\infty}^{\infty} P(v) \Phi(\Delta\nu, v) dv. \quad (15)$$

### 3. Results

Our model calculations mainly depend on three parameters: the optical thickness of the slab  $\tau_0$ , the turbulent velocity  $\sigma_t$  and the correlation length  $l$ . Due to the random nature of the velocity field, the optical thickness can not be defined uniquely. Therefore, it is characterized by the optical depth in the line center for vanishing turbulent motions,  $\sigma_t = 0$ , which is then given by  $\kappa_0 L$ .

Figure 2 demonstrates the influence of velocity correlations on the line forming process. The upper panels show the line profiles for two individual realizations of the velocity field along a given line of sight calculated with the same statistical parameters (solid curves). For comparison, also the expectation values of the intensity are shown (dashed curves). The lower panels give the corresponding optical depths  $\tau_\nu$ . In our simple model (constant density and constant pumping efficiency), the latter reflect directly the complex structure of the underlying velocity field (see Eq. [15]). Due to the exponential amplification the intensity profiles appear to have a much simpler structure than the  $\tau_\nu$ -profiles. This is in particular true if a lower intensity cut-off is introduced. Therefore do high in-

tensity spectra often consist of a single line only, which may exhibit a pronounced line shift.

As is obvious from Fig. 2 (see also Table 1), the line profiles calculated for individual realizations of the velocity field can differ substantially from each other and from the expectation value. The degree to which an individual realization can deviate from the expectation value can statistically be described by the convergence behavior of the ensemble average. We find that in general the mean value approaches the expectation value very slowly. For the chosen parameter configuration, Fig. 3 shows a sequence of averages over  $N$  realizations. Even the superposition of  $5 \times 10^5$  individual spectra is not sufficient to match the spectrum of the intensity expectation value. For a smaller correlation length or larger turbulent motions the convergence is improved but still a substantial number of profiles is required. This finding is contrary to the case of pure absorption. In the context of quasar absorption lines Levshakov et al. (1997) showed that the average of about 100 realizations reproduces the expectation value of the intensity within a one percent error margin. The radiation of an extended source reflects the average influence of the dynamical motions on the radiation field. From the above finding it can be concluded that in the case of an unsaturated maser the expectation value of the intensity will in general not be in good agreement with the measurements if a finite correlation length is involved. Even if the problem is solved self-consistently, where, due to saturation effects, the deviations from the mean intensity will be less pronounced, it can be expected that the mean intensity will not match the observations. Despite of this conclusion, the method by Traving is a valuable tool to examine the general influence of the stochastic parameters which govern the dynamical motions. It allows a very fast calculation of expectation values and distribution functions (Levshakov et al. 1997). In this respect, the method is preferable to a MC simulation which requires the generation of a very large number of realizations and is thus costly in computer time. Starting from the same model assumptions, Gail et al. (1975) examined the mean properties of the radiation field. Their most important finding is that the mean intensity increases with increasing velocity correlation. This corresponds to our result that with a larger correlation length the probability of having large peak intensities grows (see Table 1). In the present paper we want to focus on a different aspect of the problem for which the MC technique allows a more quantitative comparison of observations and model calculations. In the framework of our simple model, it is reasonable to approximate the radiation of an extended maser region by the superposition of several spectra corresponding to statistically independent lines of sight, i.e. to different realizations of the stochastic velocity field. This condition is met sufficiently if the distance between two lines of sight is larger than one correlation length. A number of  $L/l \times L/l$  lines of sight will then be adequate if the transverse extent of the region is comparable to its depth. Figure 4 shows some composite spectra of 100 realizations, with

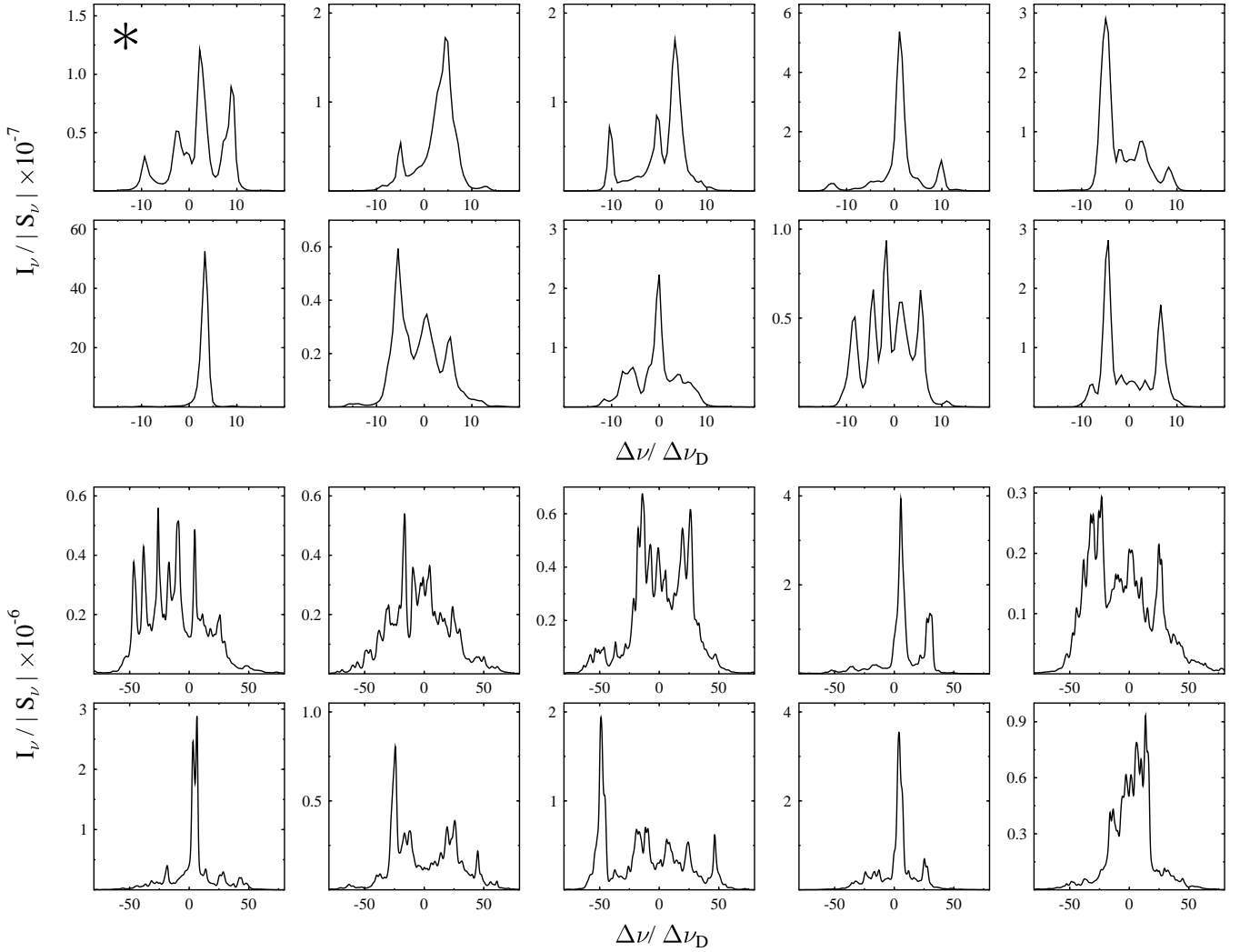


**Fig. 4.** Simulated spectra of an extended maser region. Each spectrum is composed of one hundred single realizations. In the upper ten panels we show the model calculations with a parameter set of  $l/L = 0.1$ ,  $\sigma_t/v_{\text{th}} = 10$ ,  $\tau_0 = -110$  and in the lower ten panels the parameter set is  $l/L = 0.1$ ,  $\sigma_t/v_{\text{th}} = 50$ ,  $\tau_0 = -400$ . The spectrum marked by an asterisk is used in Fig. 8

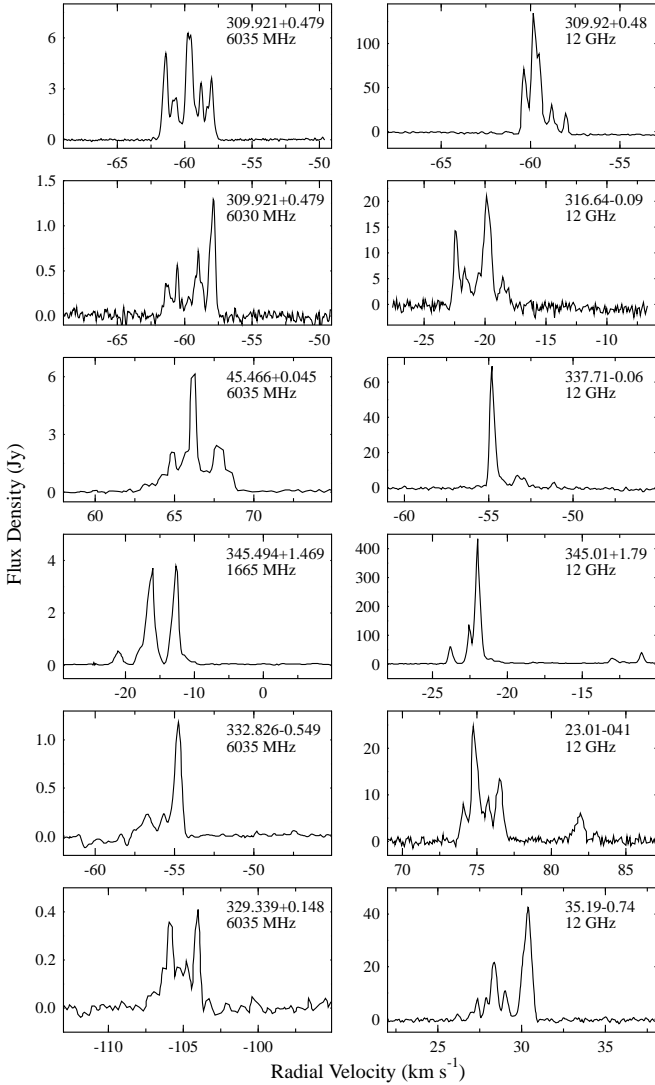
**Table 1.** For various correlation length the probability that the maximum intensity of an individual random spectrum exceeds a certain value is given. For all cases the peak intensities are compared to the intensity expectation value in the line center as calculated from the parameter configuration given in Fig. 2

Greater than	$L/l = 10$	$L/l = 25$	$L/l = 50$
$0.1 \cdot \langle I_{\Delta\nu=0} \rangle$	69.2%	37.3%	15.7%
$1 \cdot \langle I_{\Delta\nu=0} \rangle$	28.0%	3.5%	0.13%
$10 \cdot \langle I_{\Delta\nu=0} \rangle$	6.5%	0.06%	0.0%
$100 \cdot \langle I_{\Delta\nu=0} \rangle$	0.9%	0.0%	0.0%

$l/L = 0.1$  and  $\sigma_t = 10 \times v_{\text{th}}$  and  $\sigma_t = 50 \times v_{\text{th}}$  respectively. It should be emphasized that these spectra are not

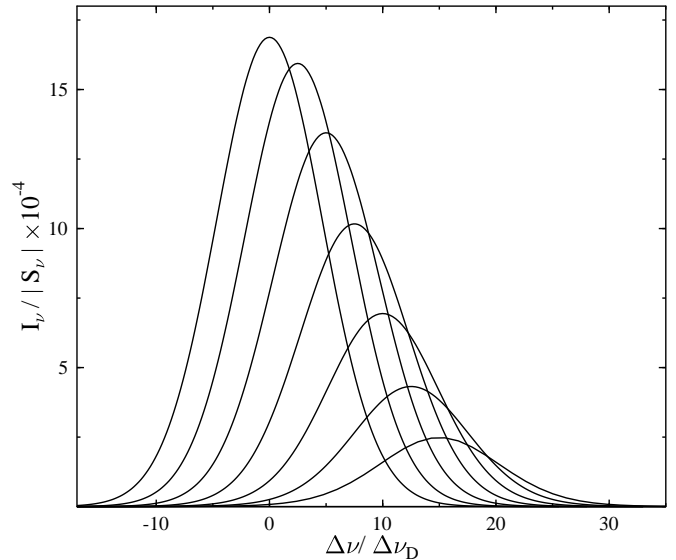
selected by predefined criteria but are randomly chosen. It is conspicuous that they exhibit a distinct structure which is far from the spectrum of the intensity expectation value. They show pronounced maxima spreading partly over a frequency range of more than  $2 \times \sigma_t$ . In the standard analysis they would be attributed to several independent sources at different radial velocities. As mentioned before, the spiky structure of the spectra is caused by the correlations in the velocity field. It should be noted, however, that - due to the exponential amplification - the intensity distribution does not reflect directly the velocity distribution (see Fig. 2 in which the optical depth is proportional to the projected velocity distribution).

Figure 5 shows a selected sample of observed *OH* and *CH<sub>3</sub>OH* maser spectra obtained by J. Caswell (private communication). A detailed description of most sources can be found in Caswell (1993, 1998, 2001) together with additional maser spectra. Our simple model does clearly



**Fig. 5.** A sample of selected *OH* (left column) and *CH<sub>3</sub>OH* (right column) maser spectra observed by J. Caswell. All sources are associated with star forming regions or ultra compact H II regions. Methanol masers are in general negligibly polarized which makes them particularly suitable for a comparison with our synthetic spectra. Except of the two spectra of the source 309.921+0.479 which are lefthanded polarized the polarization of all other *OH* sources is unknown

not allow a detailed analysis of the observations. However, it is remarkable that it can reproduce the characteristic structure of the observed line profiles. Also the velocity scale of our model spectra is in agreement with the observations, if for example, a typical cloud temperature of 25 K is assumed. In this case the thermal velocity of the *OH* and *CH<sub>3</sub>OH* molecules is  $v_{\text{th}}(\text{OH}) = 0.156 \text{ km s}^{-1}$  and  $v_{\text{th}}(\text{CH}_3\text{OH}) = 0.114 \text{ km s}^{-1}$ , respectively. Due to the higher velocity dispersion, the spectra in the lower panels of Fig. 4 show a richer structure and span a larger velocity range than the spectra in the top panels. Of course, also the amplification of radiation is affected by larger velocity differences along a line of sight. Therefore, we had to



**Fig. 6.** Expectation values of the intensity calculated for an expanding plane parallel slab with a constant velocity gradient of  $dv_{\text{sys}}/ds = 0, 5, 10, 15, 20, 25, 30 v_{\text{th}}/L$  (in decreasing order). All other parameters are the same as in Fig. 2

choose for both models very different opacity parameters to achieve the typical spiky structure of maser profiles.

In this context, one may also ask how an additional systematic velocity field influences the line formation. For this purpose we considered an expanding plane parallel slab with a constant systematic velocity gradient superposed on the stochastic velocity field. The general effect of this modification of our model can be viewed in Fig. 6 where the expectation value of the intensity for various values of the expansion velocity is shown (solid lines). As expected, this additional velocity component leads on average to a weakening of the radiated emission and to a shift of the velocity distribution function. Additionally, a slight broadening of the profile of the intensity expectation value is seen. Its width gives directly an estimation of the velocity range over which individual random spectra will be distributed. The shape of individual line profiles is very sensitive to changes of the velocity field. In Fig. 7 we model again the radiation of a maser region by a superposition of  $L/l \times L/l$  lines of sight. The turbulent velocity field is in all cases the same and only the strength of the linear expansion differs. From this example it is obvious that even small outflow velocities can significantly change the appearance of the resulting spectra. The tendency that with increasing systematic motions the emission is reduced is also clearly seen. But the gradients of the systematic and the turbulent velocity field can also partly compensate each other, allowing a strong amplification of radiation along particular lines of sight. This behavior is seen in the sequence  $dv_{\text{sys}}/ds = 0, 1, 2, 4 v_{\text{th}}/L$  and in the case  $dv_{\text{sys}}/ds = 20 v_{\text{th}}/L$ .

It is also instructive to simulate the spatial intensity distribution of composite spectra. As described before the

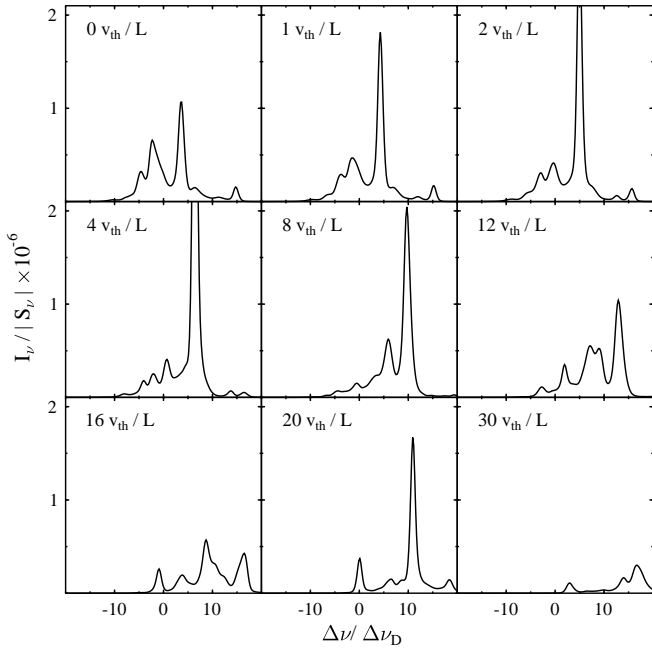


**Fig. 7.** As in Fig. 4 the spectra model the emission of an extended maser region with the parameter configuration:  $l/L = 0.1$ ,  $\sigma_t/v_{th} = 10$ ,  $\tau_0 = -110$ . For all calculations the same turbulent velocity field was used. Additionally we consider along the line of sights a systematic velocity component with a constant velocity gradient  $dv_{sys}/ds$ . The values used in each calculation are shown in the upper left corner of the panels

emerging radiation from our model cloud is approximated by the superposition of  $L/l \times L/l$  independent lines of sight corresponding to individual realizations of the velocity field. The general characteristics of the spatial intensity map of the cloud's surface can be simulated by distributing the maximum intensity found in each contributing spectrum randomly on a square grid of  $L/l \times L/l$  cells. In Fig. 8 we consider as an example the spectrum marked with an asterisk in Fig. 4. The black circles indicate maximum intensities greater than ten times the expectation value in the line center. Their number corresponds to the number of distinct spectral components. The grey and white circles show maximum intensities in the range between  $10 \langle I_{\nu=0} \rangle \geq I_{\nu,max} \geq \langle I_{\nu=0} \rangle$  and  $\langle I_{\nu=0} \rangle \geq I_{\nu,max} \geq 0.1 \langle I_{\nu=0} \rangle$  respectively. The maximum intensity in the blank boxes is below one tenth of the expectation value of the intensity in the line center. Due to the underlying stochastic velocity field, large spatial intensity variations are seen. Similar to observed high resolution intensity maps the maser region consists of a few strong sources at different radial velocities (see, e.g., Reid et al. 1980), while the radiation from most of the region is inconspicuous.

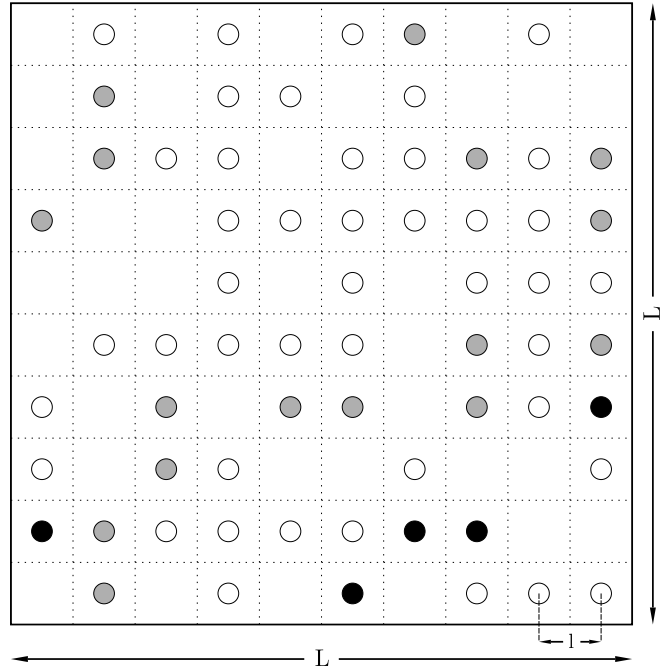


**Fig. 8.** Spatial intensity distribution of the spectrum in Fig.4 marked with an asterisk. Black circles indicate a maximum intensity of a single realization greater than ten times the expectation value in the line center. Grey and white circles show maximum intensities in the range between  $10 \langle I_{\nu=0} \rangle \geq I_{\nu,max} \geq \langle I_{\nu=0} \rangle$  and  $\langle I_{\nu=0} \rangle \geq I_{\nu,max} \geq 0.1 \langle I_{\nu=0} \rangle$  respectively. The intensity in the blank boxes is below one tenth of the mean intensity in the line center

## 4. Conclusion

In the previous sections we have investigated the influence of a turbulent velocity field with finite correlation length on the appearance of a cosmic maser source. For this, we used a very simple stochastic model in which the only spatially varying quantity is the hydrodynamical velocity, while all other parameters, in particular the density and the pump efficiency are held constant. With this simple model, we could to a surprisingly high degree reproduce the observed characteristics of cosmic masers, in particular those related to star forming regions. Our results are a strong indication that the details of the hydrodynamic velocity field inside a maser region are of great importance for the interpretation of the observed properties of the source. Of course, reality is considerably more complex than our simple model. It is very likely that in star forming regions not only the velocity is a fluctuating quantity, but also the density and other physical parameters determining the pump efficiency show strong spatial variations. However, our results convincingly show that the observation of a maser spot, by itself does not necessarily imply that the physical conditions at the location of the spot are peculiar. The spot may as well be the result of the details of the velocity distribution along the line of sight.

In view of the simplicity of our model, we have made no attempt to compare results in more detail with observa-

tional results of particular maser regions. Such attempts, however, have been performed by other authors investigating effects of turbulent motions on maser spectra. The approach closest to ours is that of Sobolev et al. (1998). They consider also a slab which is homogeneous except for the velocity field. The latter is characterized by its statistical properties. From these, individual realizations of the velocity field are constructed which then are used to calculate the optical depth and the emitted spectrum. Their approach differs from ours in the assumptions about the velocity field and in the numerical procedure. For the velocity field they assume a more general power spectrum

$$P_3(k) \sim \frac{k^2}{(k_{\min}^2 + k^2)^\alpha}, \quad (16)$$

where  $k_{\min}$  has been introduced to avoid divergence for  $k \rightarrow 0$ . Physically,  $k_{\min}$  is identified with the inverse of the linear size of the emitting volume. (In our case this identification would correspond to the assumption  $l/L = 1$ .) To construct individual realizations of the velocity field random sampling is done in k-space (for details see Dubinski et al., 1995) and the velocity field is then obtained by a Fourier transformation. Sobolev et al. investigate in particular models with  $\alpha$  close to 17/6. The case  $\alpha = 17/6$  corresponds to a Kolmogorov spectrum, which is the common approximation for turbulence in an incompressible fluid. The general result obtained by Sobolev et al. is similar to ours: The spiky structure of maser spectra and the concentration of the emitted radiation in narrow bright spots, may be caused solely by the velocity field. - They then compare their results with detailed observations of the methanol masers in OMC-1. They find evidence that the power spectrum of the turbulence in OMC-1 is somewhat steeper than an actual Kolmogorov spectrum and conclude that  $\alpha \geq 3$ . (With  $\alpha = 3$  the spectrum (16) approaches (7) in the limit  $k \rightarrow \infty$ ) - We note in passing that for this more general velocity field there exists no generalized radiative transfer equation as was derived by Traving and associates (Gail et al. 1974, Traving 1975) for the special correlation function (3). I.e., if one is interested in the expectation value of the spectrum, one actually has to calculate the average of a sufficiently large number of spectra for individual realizations. In the case of maser emission this number may be very large, as shown in Fig. 3.

A very different approach is followed by Gwinn (1994a,b). He tries to solve the inverse problem, i.e. he attempts to derive the characteristics of the velocity field directly from the very detailed observations available for the  $H_2O$  maser region in W49N. The observations are interpreted by a model in which a strong stellar wind strikes ambient material and the arising shocks provide the excitation energy for the masers. More than 250 maser features were identified. Gwinn measures the distribution of the individual maser spots in coordinate and velocity space. From the derived power law correlation functions he concludes that the velocity field in the maser region is turbulent. This interpretation of the observations makes the (implicit) assumption that the velocities of the individual

maser spots reflect directly the velocity field in the maser region. This assumption is appropriate if one considers the maser spots as physical entities like clumps. If one considers models like ours or that of Sobolev et al. (1998), in which the maser spots are solely caused by the correlations in the velocity field, the situation is more complex (see Fig. 2). - A similar statistical analysis of high quality observational data for the  $H_2O$  masers in the star forming regions Sgr B2(M), W49N, W51(MAIN), W51N, and W3(OH) has been performed by Strelnitski et al. (2002). They find that the two-dimensional distribution of maser spots shows a fractal structure and that the two-point velocity structure functions can be approximated by power laws with exponents close to Kolmogorov's values. From these findings they conclude that the velocity field in these maser regions is highly turbulent.

*Acknowledgements.* We thank Dr. James Caswell for providing the observed maser spectra shown in Fig. 5 and for many interesting discussions. We also acknowledge constructive comments of the referee Dr. C. R. Gwinn, as well as discussions with Dr. B. Deiss and C. Hengel on the different types of correlation functions and power spectra.

This research has been partly supported by the BMBF/DLR under Grant No. 50 OR 0203.

## References

- Caswell, J. L. 1993 MNRAS, 260, 425
- Caswell, J. L. 1998 MNRAS, 297, 215
- Caswell, J. L. 2001 MNRAS, 326, 805
- Dubinski, J., Narayan, R., & Phillips, T. G. 1995, APJ 448, 226
- Gail, H.-P., Hundt, E., Kegel, W. H., Schmid-Burgk, J., & Traving, G. 1974, A&A, 32, 65
- Gail, H.-P., Kegel, W. H., & Sedlmayr, E. 1975 A&A, 42, 81
- Gail, H.-P., Sedlmayr, E., & Traving, G. 1980 JQRST, 23, 267
- Gwinn, C. R. 1994a APJ 429, 241
- Gwinn, C. R. 1994b APJ 429, 253
- Levshakov, S. A., & Kegel, W. H. 1994, MNRAS, 271, 161
- Levshakov, S. A., Kegel, W. H., & Mazets, I. E. 1997, MNRAS, 288, 802
- Reid, M. J., Haschick, A. D., Burke, B. F. et al. 1980, APJ, 239, 89
- Sobolev, A. M., Wallin, B. K., & Watson, W. D. 1998, APJ 498, 763
- Strelnitski, V., Alexander, J., Gezari, S. et al. 2002, APJ 581, 1180
- Traving, G. 1975, in Baschek, B., Kegel, W. H., & Traving, G., eds. Problems in Stellar Atmospheres and Envelopes (Springer, Berlin), 326